

S₃: A Spectral and Spatial Measure of Local Perceived Sharpness in Natural Images

Cuong T. Vu, Thien D. Phan, and Damon M. Chandler

Abstract—This paper presents an algorithm designed to measure the local perceived sharpness in an image. Our method utilizes both spectral and spatial properties of the image: For each block, we measure the slope of the magnitude spectrum and the total spatial variation. These measures are then adjusted to account for visual perception, and then, the adjusted measures are combined via a weighted geometric mean. The resulting measure, i.e., S₃ (spectral and spatial sharpness), yields a perceived sharpness map in which greater values denote perceptually sharper regions. This map can be collapsed into a single index, which quantifies the overall perceived sharpness of the whole image. We demonstrate the utility of the S₃ measure for within-image and across-image sharpness prediction, no-reference image quality assessment of blurred images, and monotonic estimation of the standard deviation of the impulse response used in Gaussian blurring. We further evaluate the accuracy of S₃ in local sharpness estimation by comparing S₃ maps to sharpness maps generated by human subjects. We show that S₃ can generate sharpness maps, which are highly correlated with the human-subject maps.

Index Terms—Blur, human visual system (HVS), natural scenes, sharpness, spectral slope, total variation (TV).

I. INTRODUCTION

MOST CONSUMER photographs contain particular regions that are perceived to be sharper than others. Although the term “sharpness” lacks a precise technical definition, any human can effortlessly point out the sharp regions in an image. Intuitively, a sharp region is one in which fine details are resolvable (high resolution) and in which edges and object boundaries appear to be of high contrast (high acutance [1]). Indeed, most professional photographers attempt to maximize perceived sharpness by using a high-resolution camera and employing digital retouching to increase acutance (e.g., via unsharp masking).

However, despite the ease with which perceived sharpness can be determined by eye, this task remains quite challenging for a computer. The ability to quantify the perceived sharpness of

Manuscript received March 18, 2011; revised July 12, 2011; accepted September 07, 2011. Date of publication September 29, 2011; date of current version February 17, 2012. This work was supported by the Army Research Office, “Enabling Battlefield Situational Awareness through a Cooperative and Intelligent Video Sensor Network,” W911NF-10-1-0015; and by the National Science Foundation, “Content-Based Strategies of Image and Video Quality Assessment,” Award 0917014; PI: Damon Chandler, Oklahoma State University, Stillwater. The associate editor coordinating the review of this manuscript and approving it for publication was Dr. Stefan Winkler.

The authors are with the School of Electrical and Computer Engineering, Oklahoma State University, Stillwater, OK 74078-5032 USA (e-mail: cuong.vu@okstate.edu; thien.phan@okstate.edu; damon.chandler@okstate.edu).

Color versions of one or more of the figures in this paper are available online at <http://ieeexplore.ieee.org>.

Digital Object Identifier 10.1109/TIP.2011.2169974

an image can be useful for a variety of image-processing applications. For example, autoenhancement algorithms can use this information to sharpen images in a spatially adaptive fashion [2]. Sharpness can also be a useful factor in no-reference image quality assessment (e.g., [3] and [4]) and main subject detection in photographs [5].

Previous work on sharpness estimation has largely been geared toward determining a single scalar value that quantifies the overall sharpness of an image. A common technique involves measuring the spread of edges (e.g., [3] and [4]) with the assumption that there is at least one strong edge in the image. Other techniques measure sharpness in the spectral domain based on the argument that fine detail (sharpness) is determined by high-frequency values (e.g., [2] and [6]). There are also other sharpness estimators that work in the spatial domain without any assumption regarding edges (e.g., [7] and [8]). Section II provides a review of the existing literature on image sharpness estimators.

Obtaining a single scalar estimate of sharpness for an image can be useful for tasks such as deblurring and no-reference quality assessment. Nonetheless, there are certain applications that require a map that indicates local sharpness within the image. For example, in main-subject detection, objects that are sharp are usually considered as candidates of the main subjects; thus, a local sharpness map can be an effective feature [5]. Although it is possible to modify existing sharpness estimators to operate in a block-based fashion to generate a sharpness map, we seek a technique that is specifically designed for such local sharpness estimation.

In this paper, we propose an algorithm that can measure the perceived sharpness of local image regions and does not require the presence of edges. Indeed, images commonly contain both edges and textures, and it is often the textures that appear sharper than the edges (e.g., a seashell in the sand). Our measure is based on two factors: 1) a spectral measure based on the slope of the local magnitude spectrum and 2) a spatial measure based on local maximum total variation (TV). Our work draws on the concepts proposed by Shaked and Tastl [2] and Field and Brady [9] (spectral aspect) and on the concept of TV proposed by Rudin *et al.* [10] and Blanchet *et al.* [11] (spatial aspect).

It is well known that the attenuation of high-frequency content can lead to an image that appears blurred. One way to measure this effect is to examine the image’s magnitude spectrum $M(f)$, which is known to fall inversely with frequency, i.e., $M(f) \propto f^{-\alpha}$, where f is the frequency and $-\alpha$ is the slope of the line $\log M \propto -\alpha \log f$ (see Section III-A for details about the computation of the magnitude spectrum). For natural scenes, α is typically in the range of 0.7–1.6 [12]. Researchers have argued that the human visual system (HVS) is tuned to

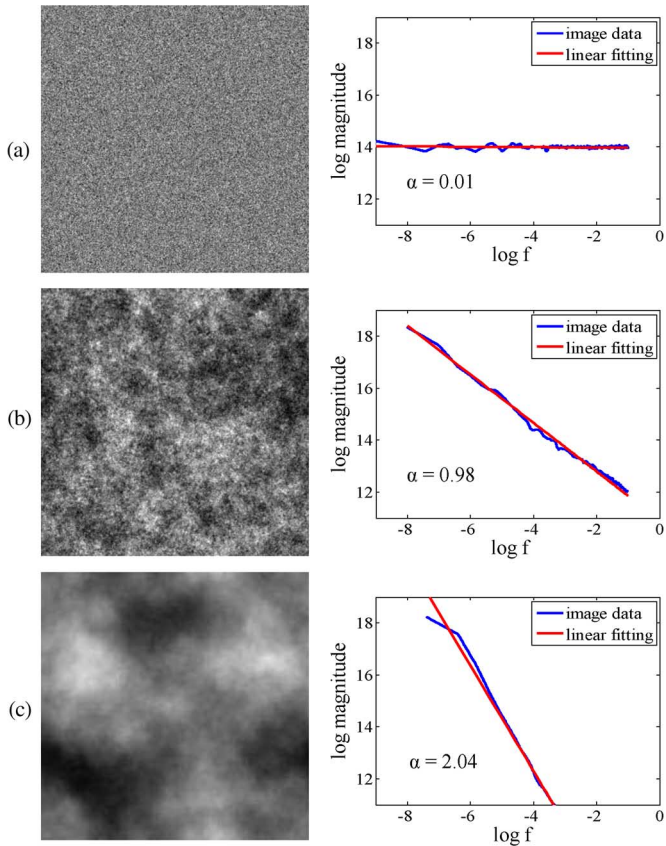


Fig. 1. Noise images with different slope factors (see Section III-A for details about measuring the slope of magnitude spectrum).

this characteristic natural-scene spectrum [13]. An increase in α corresponds to a steeper line, indicating a relative reduction in high-frequency content and, thus, a potential reduction in perceived sharpness. Our spectral measure of sharpness follows from the argument put forth by Field and Brady [9]: An image region whose spectrum exhibits a slope factor of $0 \leq \alpha \leq 1$ will appear sharp, whereas regions with $\alpha > 1$ will appear progressively blurred as α increases. Examples to support this argument are shown in Fig. 1. This figure shows noise images whose spectra have different slope values. The white noise image, with a slope of 0, appears very sharp, whereas the Brownian noise image (which is also called red noise or $1/f^2$ noise) appears very smooth. The pink noise, on the other hand, is somewhat in between; it is almost as sharp as the white noise and clearly much sharper than the $1/f^2$ noise image.

While the slope of the magnitude spectrum can be a potential measure of sharpness, it does not take into account contrast, which is known to affect perceived sharpness [14]. Two images can have the same spectral slope but appear to be of different sharpnesses due to a difference in contrast. Fig. 2 demonstrates this assertion. The low-contrast image in Fig. 2(b) was generated from Fig. 2(a) by taking 40% of the value of every pixel in (a) and then adding a constant to the resulting image to make both images have the same mean luminance. The magnitude spectrum of Fig. 2(b) (ignoring the dc component) is therefore proportional to that of (a); thus, both images have the same slope factor. However, the image in (a) appears much sharper than (b) due to the low contrast of the latter (see Fig. 2's caption and the

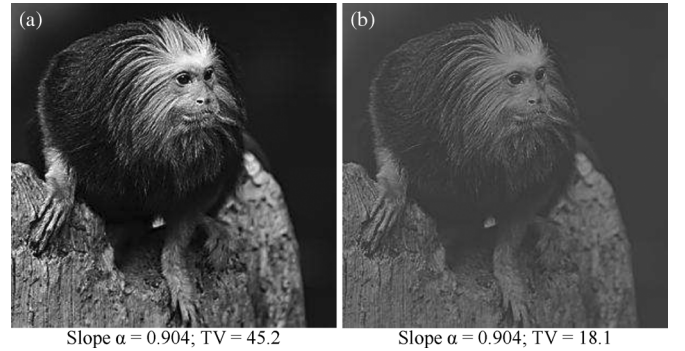


Fig. 2. Slope of the magnitude spectrum does not take into account contrast. The image in (a) appears sharper than the image in (b) due to the difference in luminance contrast. Various measures of luminance contrast computed for the two images: RMS contrast (a) 1.453, (b) 0.534; Michelson contrast (a) 0.993, (b) 0.746; Weber contrast (a) 287.2, (b) 5.877. The conversion to luminance L from 8-bit pixel value I is given by $L = (0.7656 + 0.0364I)^{2.2}$, assuming the Adobe RGB color space.

online supplement to this paper [15] for various measures of luminance contrast computed for these two images).

In order to take into account contrast, we employ an additional measure in the spatial domain based on the TV [10], [11]. The TV of an image region effectively measures the sum of absolute differences between the region and a spatially shifted version of that region (see Section III-B for details about TV). Thus, a region that is smooth (e.g., sky) will exhibit a lesser TV than a region, such as a texture, which demonstrates a greater variation across space. In addition, a high-contrast region, where the differences between adjacent pixel values are high, will exhibit a larger TV than a low-contrast region. In a probabilistic framework, Blanchet *et al.* [11] have shown that TV can be used as a contrast-invariant measure of phase coherence and thereby can be used as a measure of local sharpness. We argue that a nonprobabilistic application of TV can be useful for measuring local sharpness due, in part, to its ability to take into account local contrast.

Here, we demonstrate that a weighted combination of these two measures (spectral slope and TV) can lead to an effective measure of local perceived sharpness. We have titled our sharpness estimator S_3 (*spectral and spatial sharpness*) to emphasize the fact that variations in local spectral properties and variations in local spatial properties both play a role in the perception of sharpness. The S_3 measure can yield a local sharpness map in which greater values correspond to greater perceived sharpness within an image and across different images. This S_3 map can also be collapsed into a single scalar value that denotes overall perceived sharpness for a full-sized image. We demonstrate the utility of this estimator for no-reference quality assessment of blurred images and for predicting the level of Gaussian blurring. In addition, we validate the accuracy of S_3 in local sharpness estimation by comparing S_3 maps to sharpness maps generated by human subjects.

This paper is organized as follows. Section II provides a review of the existing literature on sharpness estimation. Section III provides the details of the S_3 algorithm. In Section IV, we present results of S_3 for prediction monotonicity, quality assessment of blurred images, and correlation with subjective sharpness maps. General conclusions are presented in Section V.

II. BACKGROUND

Various algorithms have been proposed to measure the sharpness or blurriness of images. It is important to note that blurriness is not necessarily the inverse of sharpness; an unsharp region might not be blurred, and vice versa. For example, an in-focus but blank region cannot be considered sharp, nor can it be considered blurred. However, for most applications on which researchers have tested their algorithms, sharpness and blurriness have been used as antonyms. Therefore, in this paper, we review and compare our estimator to both sharpness and blurriness estimators.

Modern methods of sharpness/blurriness estimation can generally be classified into three main trends: 1) edge-based methods, which involve measuring the spread of edges; 2) pixel-based methods, which work in the spatial domain without any assumption regarding edges; and 3) transform-based methods, which work in the spectral domain. This section provides an overview of these methods.

A. Edge-Based Methods

A common technique of sharpness/blurriness estimation involves measuring the spread of edges. Indeed, edges provide a strong visual cue for judging the sharpness/blurriness of a region. A technique proposed by Marziliano *et al.* [3] is based on the smoothing effects of blur on edges. They first identify vertical edges in an image and then estimate overall blurriness based on the average edge width. Ong *et al.* [16] detected not only edges but also the gradient direction in the image. The amount of image blur is then determined as the average extent in both the gradient direction and the opposite direction of edges in the image.

Dijk *et al.* [17] first detected lines and edges in the image and then modeled the widths and amplitudes of those lines and edges as Gaussian profiles. Dijk *et al.* then quantified sharpness by using the amplitudes corresponding to the narrowest Gaussians (fifth percentile). Chung *et al.* [18] combined the standard deviation and weighted mean of the edge gradient magnitude profile to form their sharpness estimator, where the weights are obtained from the contrast of the image. Assuming that at least one sharp edge can be detected, Wu *et al.* [19] constructed the line spread function and thus extracted the point spread function (PSF). The radius of the PSF is used as the degree of blurriness of the image. In addition to detecting the local edge strength in the image, Zhong *et al.* [20] proposed a sharpness estimator that also utilizes the information from the corresponding saliency map, which is obtained via their saliency model.

Ferzli and Karam [4] introduced the notion of just noticeable blur (JNB). The JNB is defined as the threshold with which a human can perceive blurriness around an edge, given a contrast higher than the just noticeable difference. The JNB concept is used to estimate the perceived blur distortion within each 64×64 edge block of the image (blocks containing a number of edge pixels greater than a threshold). The distortion for each block is then fed into a probabilistic model to estimate the perceived blur distortion of the whole image. The final sharpness index is the ratio between the total number of edge blocks in the image and the computed perceived blur distortion. Using the

concept of JNB in a different way, Narvekar and Karam [21] estimated the sharpness of an image as the cumulative probability of detecting blur at an edge.

B. Pixel-Based Methods

There are also sharpness/blurriness estimators that work in the spatial domain and do not make assumptions about the edges in the image. Wee and Paramesran [8] argued that the eigenvalues of an image contain information about the maximum variance in that image, and thus, the dominant eigenvalues can be used to estimate sharpness. They first compute the eigenvalues of the covariance matrix of the image and then take the trace of the first several eigenvalues as the image sharpness index. Using a similar approach [22], Zhu and Milanfar estimated sharpness based on the singular value decomposition of the local image gradient matrix. Their argument is that the singular values are sensitive to sharpness because they reflect the strength of the gradients along the dominant direction and its perpendicular direction. Therefore, the singular values of the local image gradient matrix can be used to estimate sharpness.

Crete *et al.* [23] generated a blurred version of the input image and then computed the variation between neighboring pixels of each image. The blurriness of the original image is estimated based on a comparison of the two variations. Tsomko and Kim [24] proposed a blur estimator that operates by using the variance of the prediction residue, which is computed as the difference between adjacent pixels. Debing *et al.* [25] focused on measuring the blurring artifacts from H.264/AVC compression. Their blur index is averaged from all the local blur values calculated at the boundaries of macro blocks.

C. Transformed-Based Methods

A number of sharpness/blurriness algorithms work in the spectral domain using transforms such as the discrete cosine transform (DCT) or discrete Fourier transform (DFT). Marichal *et al.* [26] estimated sharpness based on the histogram of nonzero DCT coefficients among all 8×8 blocks of the transformed image. In addition, using the DCT, Caviedes and Gurbuz [6] built a block-based sharpness estimator using the kurtosis of the DCT coefficients of each block; the overall sharpness estimate is given by the average of the sharpness values computed for edge profiles. Zhang *et al.* [27] argued that the sharpness of an image is closely related to the peakedness of its power spectral density. Therefore, they estimated the sharpness based on the kurtosis of the power spectral density of the image.

Shaked and Tastl [2] estimated sharpness using a technique based on the ratio of high- to low-pass frequency energy of the spatial derivative of each line/column. Kristan *et al.* [28] measured the uniformity of the image spectrum as their estimate of sharpness. In order to reduce computational complexity, Kristan *et al.* divided the image into 8×8 blocks and then used the DCT to estimate the spectra. Hassen *et al.* [29] measured sharpness based on local phase coherence (LPC) in the complex wavelet domain. They computed the LPC at each spatial location to build an LPC map and then computed an overall sharpness index via a weighted sum of the values in the LPC map using weights determined by the rank order of these values.

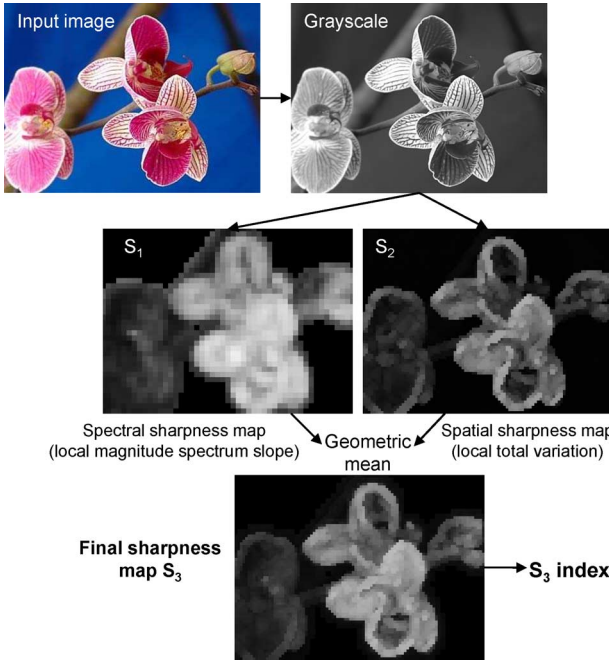


Fig. 3. Outline of the S_3 algorithm. The input color image is first converted into grayscale. The sharpness measure based on the spectral slope S_1 and the sharpness measure based on the local TV S_2 are combined into the final sharpness map S_3 . The S_3 map is then collapsed into a single value S_3 index, which quantifies the overall perceived sharpness of the whole image.

III. ALGORITHM

In this section, we describe the operation of the S_3 algorithm, an outline of which is shown in Fig. 3. As mentioned in Section I, two estimators of sharpness are employed: 1) a spectral-based estimator, which operates based on the slope of the local magnitude spectrum; and 2) a spatial-based estimator, which operates based on local TV. We refer to these two estimators as S_1 and S_2 , which result in maps called the S_1 map and S_2 map, respectively. The final estimate of local sharpness is computed by combining the S_1 and S_2 maps into a third map, which we call the S_3 map. The S_3 map can be collapsed into a single value, i.e., the S_3 index, which quantifies the overall perceived sharpness of the whole image.

Let \mathbf{X} denote the $M_1 \times M_2$ -pixel grayscale image, which will serve as the input to both the S_1 and S_2 measures. If the input is a color image, we first convert it to grayscale via a pixel-wise transformation of

$$\mathbf{X} = 0.2989\mathbf{R} + 0.5870\mathbf{G} + 0.1140\mathbf{B} \quad (1)$$

where \mathbf{R} , \mathbf{G} , and \mathbf{B} denote the 8-bit red, green, and blue intensities, respectively. We divide \mathbf{X} into blocks of size $m \times m$ pixels with d pixels of overlap between neighboring blocks. Let \mathbf{x} denote a block of \mathbf{X} .

A. S_1 : Spectral Measure of Sharpness

Our spectral measure of sharpness follows from the argument put forth by Field and Brady [9]: An image region whose magnitude spectrum exhibits a slope factor of $0 \leq \alpha \leq 1$ will appear sharp, whereas regions with $\alpha > 1$ will appear progressively less sharp as α increases. Here, we estimate α for each image block \mathbf{x} by using the local magnitude spectrum, and then, we

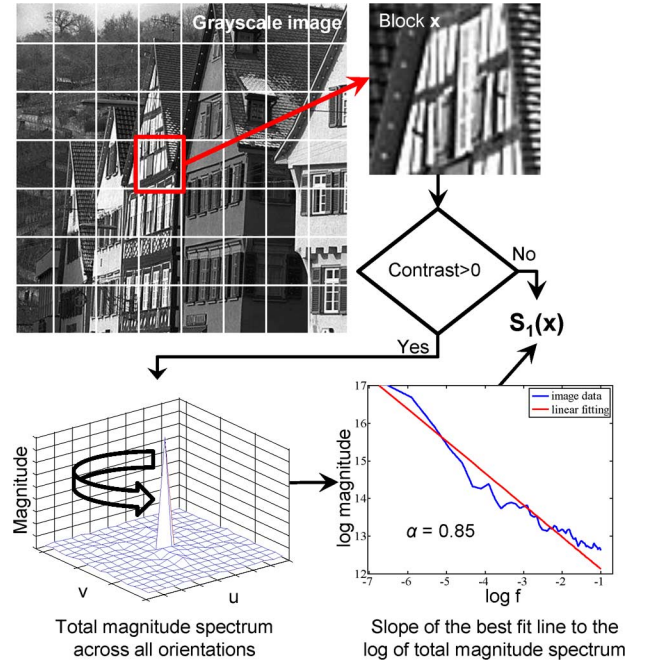


Fig. 4. Diagram of the S_1 measure. For each block \mathbf{x} , $S_1(\mathbf{x})$ is computed based on the slope of its magnitude spectrum.

employ a transducer function derived from Field and Brady's claim (see [30] for a theoretical account of the claim).

Let $S_1(\mathbf{x})$ denote a measure of the perceived sharpness based on the spectral slope of block \mathbf{x} . An outline of the S_1 measure is shown in Fig. 4. For each block, we first check if the contrast of \mathbf{x} is effectively zero, in which case $S_1(\mathbf{x})$ is set to zero for that block. The contrast of \mathbf{x} is considered to be zero if $\max(\mathbf{l}(\mathbf{x})) - \min(\mathbf{l}(\mathbf{x})) \leq T_1$ or $\mu_{\mathbf{l}(\mathbf{x})} \leq T_2$, where $\mu_{\mathbf{l}(\mathbf{x})}$ denotes the mean of $\mathbf{l}(\mathbf{x})$ and $\mathbf{l}(\mathbf{x}) = (b + k\mathbf{x})^\gamma$ denotes the luminance-valued block, with $b = 0.7656$, $k = 0.0364$, and $\gamma = 2.2$, assuming the Adobe RGB display conditions. Thresholds $T_1 = 5$ and $T_2 = 2$ were chosen empirically, assuming the input block contains pixel values in the range of 0–255.

When the contrast of \mathbf{x} is greater than zero, $S_1(\mathbf{x})$ is computed based on the slope of the magnitude spectrum of \mathbf{x} . Specifically, we compute the 2-D DFT of \mathbf{x} denoted $\mathbf{y}_x(f, \theta)$, where f is the radial frequency and θ is the orientation. The quantities f and θ can be computed from the DFT indices $u \in [-m/2, m/2]$ and $v \in [-m/2, m/2]$ via

$$f = \left[\left(\frac{u}{m/2} \right)^2 + \left(\frac{v}{m/2} \right)^2 \right]^{1/2} \quad (2)$$

$$\theta = \arctan \left(\frac{v}{u} \right). \quad (3)$$

We next compute the magnitude spectrum summed across all orientations $\mathbf{z}_x(f)$, as given by

$$\mathbf{z}_x(f) = \sum_{\theta} |\mathbf{y}_x(f, \theta)|. \quad (4)$$

The slope of the magnitude spectrum of \mathbf{x} denoted as $-\alpha_x$ is computed as the slope of the line in the form $-\alpha \log f + \log \beta$,

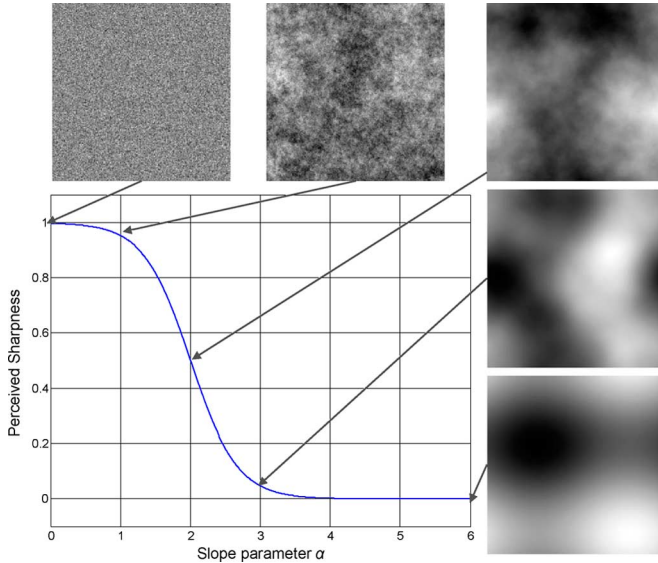


Fig. 5. Relationship between perceived sharpness and slope parameter α .

which best fits to the log of the total magnitude of \mathbf{x} . Specifically, $\alpha_{\mathbf{x}}$ is computed via

$$\alpha_{\mathbf{x}} = \arg \min_{\alpha} \|\beta f^{-\alpha} - \mathbf{z}_{\mathbf{x}}(f)\|_2^2 \quad (5)$$

where the L_2 -norm is taken over all radial frequency $f > 0$. Generally, a larger value of $\alpha_{\mathbf{x}}$ denotes less higher frequency content compared to lower frequency content. Finally, $S_1(\mathbf{x})$ is given by

$$S_1(\mathbf{x}) = 1 - \frac{1}{1 + e^{\tau_1(\alpha_{\mathbf{x}} - \tau_2)}} \quad (6)$$

where $\tau_1 = -3$, and $\tau_2 = 2$. Here, a sigmoid transducer function, which was motivated by Field and Brady's claim [30], is employed to estimate the perceived sharpness from $\alpha_{\mathbf{x}}$. This sigmoid, as shown in Fig. 5, attempts to account for the tuning of the HVS to the spectrum of natural scenes, i.e., regions with a slope factor of $0 \leq \alpha \leq 1$ appear sharp, whereas regions with $\alpha > 1$ appear blurred. Notice from the noise images in Fig. 5 that the perceived sharpness changes slowly for $\alpha \in [0, 1]$, changes rapidly for $\alpha \in [1, 3]$, and saturates for $\alpha > 3$. The two parameters τ_1 and τ_2 were chosen by fitting a sigmoid to subjective ratings of sharpness (using the authors as subjects) for the noise images shown in Fig. 5; the final values of $\tau_1 = -3$ and $\tau_2 = 2$ were rounded from the raw parameters of the fitted sigmoid (see [15] for an analysis of how perturbations of τ_1 and τ_2 affect the performance of S_3).

In applying Equations (2)–(6), we use blocks of size $m = 32$ and an overlap of $d = 24$. We have found that this relatively large block size of $m = 32$ provides a sufficient number of DFT coefficients to accurately estimate the slope of the local spectrum. We also use a Hanning window denoted by $\mathbf{w} = [w_1, w_2, \dots, w_m]^T$, whose k th entry is given by

$$w_k = 0.5 \left(1 - \cos \left(\frac{2\pi k}{m+1} \right) \right) \quad (7)$$

to suppress edge effects in the Fourier analysis. To apply \mathbf{w} to each block \mathbf{x} , we create a 2-D version of \mathbf{w} by using an outer product; thus, each block is windowed by performing point-by-

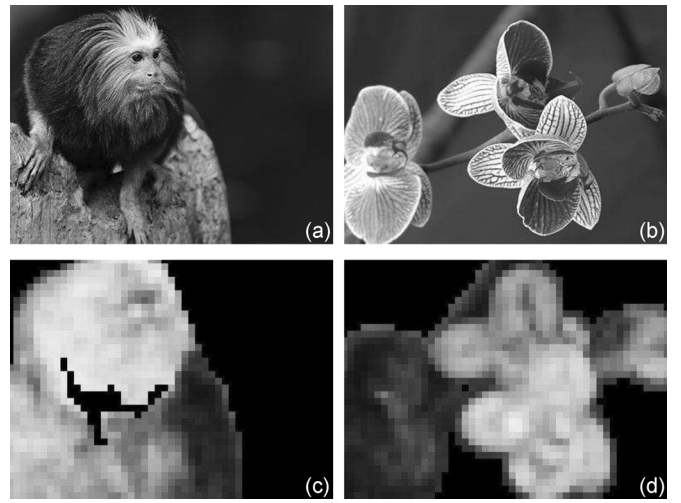


Fig. 6. (a) and (b): input images; (c) and (d): corresponding S_1 maps in which brighter blocks denote greater perceived sharpness.

point multiplication of \mathbf{x} with $\mathbf{w}\mathbf{w}^T$. The $S_1(\mathbf{x})$ values for all blocks are assembled to form our spectral-based sharpness map denoted by $S_1(\mathbf{X})$.

Fig. 6 shows S_1 maps of several images. For the image *monkey* in Fig. 6(a), the corresponding S_1 map is able to capture some sharp regions such as the white fur in the left side of the monkey's eyes and in the monkey's right hand. This S_1 map also correctly assigns low sharpness values to blurred regions such as the background and the part of the rock in the right-hand side of the image. For the image *orchid* in Fig. 6(b), the sharpest regions occur both inside the middle orchids' petals and their borders. The petals from the orchid on the left, on the other hand, are more blurred. The corresponding S_1 map of this image can also capture these facts.

Fig. 6 also demonstrates that S_1 does indeed fail on some regions. In the image *monkey*, the rock under the monkey's right hand does not appear to be as sharp as the map indicates. Similarly, the fur closest to the monkey's mouth does not appear quite as sharp as indicated by the map. In the image *orchid*, the sharpness of the interior of the flower bud on the right side of the image and the interior of the lowest petal of the middle orchid are also overestimated. Most of these failures are due to the fact that the slope of the spectrum does not take into account contrast. In order to handle this fact, we also employ a spatial measure of sharpness S_2 as a second estimator of local perceived sharpness.

B. S_2 : Spatial Measure of Sharpness

For our spatial-based measure of sharpness, we employ a modified version of the TV proposed in [11]. A block diagram of the spatial measure of sharpness S_2 is shown in Fig. 7(a). The TV of block \mathbf{x} , which is denoted by $v(\mathbf{x})$, is given by

$$v(\mathbf{x}) = \frac{1}{255} \sum_{i,j} |x_i - x_j| \quad (8)$$

where x_i and x_j are 8-neighbor pixels in \mathbf{x} .

The TV $v(\mathbf{x})$ effectively measures the sum of absolute differences between \mathbf{x} and a spatially shifted version of \mathbf{x} . Therefore,

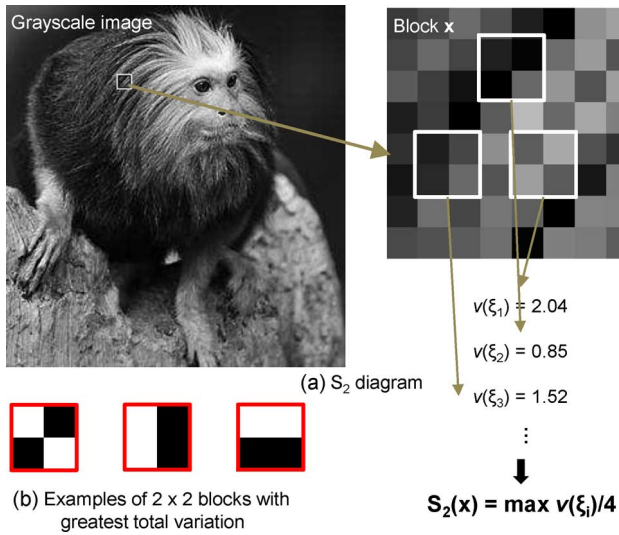


Fig. 7. (a) Diagram of the S_2 measure. The greatest possible TV of a 2×2 block is 4; examples of such blocks are shown in (b).

if x is of high contrast, then the differences between adjacent pixel values are high; thus, (8) will yield a larger TV than it would for a lower contrast block.

Let $S_2(x)$ denote the measure of perceived sharpness based on the TV of block x . Instead of deriving $S_2(x)$ directly from the TV of x , we compute it as the maximum of the TV of smaller blocks of x via

$$S_2(x) = \frac{1}{4} \max_{\xi \in x} v(\xi) \quad (9)$$

where ξ is a 2×2 block of x .

The max operator used in (9) attempts to account for visual summation across space [31]. That is, the HVS combines perceptual responses across space in a nonlinear fashion, which has been shown to be well approximated via a max operator (L_∞ -norm). Because the greatest TV of a 2×2 block is 4, the coefficient 1/4 attempts to normalize $S_2(x)$ to lie in the range of 0–1. (Examples of 2×2 blocks with the greatest TV are shown in Fig. 7(b).) For this local TV measure, we use blocks of size $m = 8$ with $d = 4$ pixels of overlap between blocks. The $S_2(x)$ values for all blocks are assembled to form our spatial-based sharpness map denoted by $S_2(\mathbf{X})$.

The S_2 maps of the images *monkey* and *orchid* are shown in Fig. 8. For the image *monkey* in Fig. 8(a), the monkey has very sharp eyes, a sharp nose, and a sharp right hand, which are observations that are correctly reflected in the corresponding S_2 map. Blurred regions such as the background and the part of the rock in the right-hand side of the image are again accurately detected by S_2 . The S_2 map of the image *orchid* is also able to capture sharp regions such as the middle orchids' borders, and it correctly assigns low sharpness values to the leftmost blurred orchid and to the blurred background.

In Fig. 6, we demonstrated that S_1 fails in some low-contrast regions. Fig. 8 shows that S_2 works better than S_1 for these regions. The S_2 measure assigns low sharpness values to some regions for which S_1 overestimates the sharpness, e.g., the regions around the mouth of the monkey, the inside area of the flower

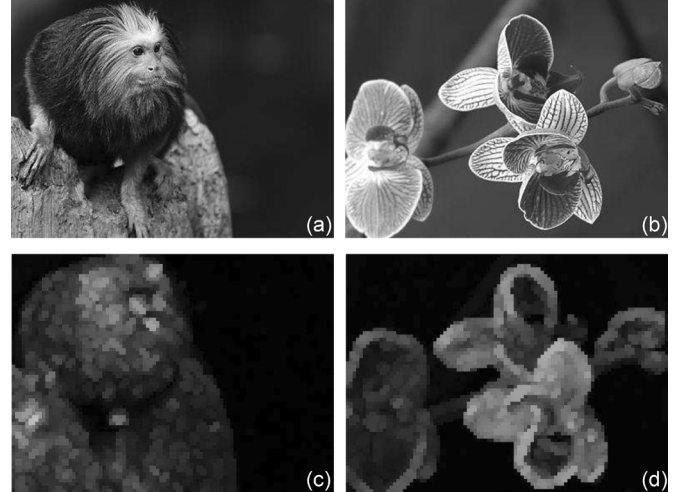


Fig. 8. (a) and (b): input images; (c) and (d): corresponding S_2 maps in which brighter blocks denote greater perceived sharpness.

bud, and the interior of the lowest petal of the middle orchid. However, S_2 alone shows a weakness in working with textures. For example, the monkey contains very sharp fur, whereas S_2 underestimates the sharpness of this region. Together, S_1 and S_2 can generally compensate for each other's failures. As described next, our overall sharpness map S_3 utilizes a combination of S_1 and S_2 .

C. Combining the Spectral and Spatial Measures

We combine the spectral-based sharpness map $S_1(\mathbf{X})$ and the spatial-based sharpness map $S_2(\mathbf{X})$ into an overall perceived sharpness map $S_3(\mathbf{X})$ by using a weighted geometric mean

$$S_3(\mathbf{X}) = S_1(\mathbf{X})^\eta \times S_2(\mathbf{X})^{1-\eta} \quad (10)$$

where $0 \leq \eta \leq 1$. We have found $\eta = 0.5$ to generally yield the best results and have accordingly used this value for the results presented in Section IV (see [15] for an analysis of the performance of S_3 with different selections of η).

When looking at two images to estimate which one is sharper, the image that appears sharper is not necessarily the one that contains more sharp regions. Instead, visual summation dictates that the overall sharpness is determined based on the sharpest region in each image. However, choosing the overall sharpness as the maximum value of the map can make the algorithm overly sensitive to spurious sharp locations due to, e.g., noise (see Section IV-E). Therefore, from the sharpness map $S_3(\mathbf{X})$, we compute the overall sharpness of \mathbf{X} by taking the average sharpness of 1% of the largest values of $S_3(\mathbf{X})$. Specifically, the S_3 index is computed via

$$S_3 = \frac{1}{N} \sum_{k=1}^N \tilde{S}_3(k) \quad (11)$$

where $\tilde{S}_3(k)$ is the k th element of the vector \tilde{S}_3 , which includes all elements from the S_3 map sorted in descending order as $\tilde{S}_3 = \text{sort}_d(S_3(\mathbf{X}))$, and where $N = \lfloor (M_1 \times M_2) / 100 \rfloor$ is the number of elements in the subset containing 1% of the largest values of $S_3(\mathbf{X})$.



Fig. 9. S_3 maps and indices for a variety of images containing common-place subject matter. The ordering of these images was determined based on subjective rankings of sharpness: (1) denotes the image ranked to be least sharp; (6) denotes the image ranked to be the most sharp.

IV. RESULTS AND ANALYSIS

In this section, we evaluate the performance of the S_3 algorithm for within-image sharpness prediction and across-image sharpness prediction. Next, we demonstrate the utility of S_3 on two tasks: no-reference quality assessment of blurred images and monotonic estimation of the standard deviation of the impulse response used in Gaussian blurring. We then describe an experiment to obtain ground-truth sharpness maps of six images. The S_3 maps of these images are compared to ground-truth maps to validate the local behavior of S_3 . Finally, we discuss the effect of Gaussian white noise on the S_3 index.

A. Representative Results

We first demonstrate, via representative results, that S_3 is able to accurately perform across-image and within-image sharpness prediction. Fig. 9 depicts S_3 maps and indices for a variety of images containing commonplace subject matter. The images in this figure have been ordered according to increasing overall perceived sharpness determined by asking eight naive subjects to rank-order the images in terms of sharpness (see [15] for details of the experiment).

In terms of across-image prediction, the S_3 index of the image *branches* is the greatest, and the blurry ball in the image *ball* has the lowest S_3 index, which agrees with the relative perceived sharpness across these images. The mountain region in the image *airplane* makes it sharper than the image *ball* but still clearly not as sharp as the image *petal*. The image *zebra* looks sharper than the image *petal* because of the sharp and high-contrast stripes in the left zebra's body. The image *pelicans* is not as sharp as the image *branches*, which contains very sharp tree branches; however, clearly, the former, in which the perceived sharpness stems from the very sharp brush, is sharper than the rest. The S_3 index is able to capture this rank ordering of overall sharpness.

In terms of within-image sharpness prediction, all of the S_3 maps quite accurately capture the sharp regions in each image. For example, in the image *ball*, the ball is blurred, which is correctly shown as dark in the map. The map is also able to point out that, in the background, the right vertical line is sharper than the left line.

As another example, the perceived sharpness of the image *zebra* stems from the high-contrast stripes of the two zebras. This fact is accurately shown in the S_3 map. Although most of the background is blurred, which correctly appears as dark in the map, the map is also able to capture the sharp bushes between the two zebras. A qualitative analysis of within-image sharpness prediction for other images is provided in [15].

B. No-Reference Quality Assessment of Blurred Images

A standard technique of quantifying the performance of a sharpness estimator is to use the algorithm for no-reference quality assessment of blurred images. To analyze the performance of S_3 on this task, we employ the blurred image subsets of three publicly available image databases: LIVE [32], CSIQ [33], and TID2008 [34] since subjective ratings of image quality in these databases are available. There are 145, 150, and 96 blurred natural images in the LIVE, CSIQ, and TID2008 databases, respectively.¹ The overall ratings of images from LIVE and CSIQ are reported as differential mean opinion scores (MOSs), whereas the ratings in TID2008 are reported as MOS. For comparison, the same sets of images were analyzed by using the following sharpness algorithms: 1) the algorithm from Marichal *et al.* (MMZ) [26]; 2) the CPBD algorithm

¹The reference images were not used for this evaluation. The authors of the LIVE database suggest to report results only for distorted images, and the reference images were not rated by subjects for CSIQ and TID2008. In addition, TID2008 contains 100 blurred images, but four blurred versions of an artificial reference image were ignored in this test.

from Narvekar and Karam [21]; 3) the JNB algorithm from Ferzli and Karam [4]; 4) the algorithm from Marziliano *et al.* (MDWE) [3]; and 5) the algorithm from Shaked and Tastl (ST) [2]. We also compare with BLIINDS-II, a no-reference image quality assessment algorithm from Saad *et al.* [35].

Before evaluating the performance of an algorithm, it is common to apply a logistic transform to the predicted ratings to bring the predictions on the same scale as the MOS or DMOS values and to account for the nonlinear relationship between the predictions and opinion scores. We adopt the logistic function suggested by the Video Quality Experts Group [36], which is given by

$$f(x) = \frac{\tau_1 - \tau_2}{1 + \exp\left(\frac{x - \tau_3}{\tau_4}\right)} + \tau_2 \quad (12)$$

where τ_1 , τ_2 , τ_3 , and τ_4 are the model parameters chosen to minimize the MSE between the predicted values and the subjective scores.

We use four criteria to compare the performances of different algorithms on the three databases: 1) Pearson correlation coefficient (CC), which measures how well an algorithm's predictions correlate with the subjective scores; 2) Spearman rank-order correlation (SROCC), which measures the relative monotonicity between the predictions and subjective scores; 3) Outlier ratio (OR); and 4) outlier distance (OD). These latter two criteria attempt to account for the inherent variation in human subjective ratings of quality, which is normally quantified by using the intersubject standard deviation σ_s of all subjective ratings for a particular image. An outlier is defined as a prediction that is outside $2\sigma_s$ of the DMOS or MOS.² Let N_{outlier} and N_{total} denote the number of outliers and the total number of predicted ratings, respectively. The OR is defined as

$$\text{OR} = \frac{N_{\text{outlier}}}{N_{\text{total}}}. \quad (13)$$

The OD, which was proposed in [33], attempts to quantify how far from the error bars ($\pm 2\sigma_s$) the outliers fall. The OD is defined as

$$OD = \sum_{x \in X_f} \min(|f(x) - s(x) - 2\sigma_s|, |f(x) - s(x) + 2\sigma_s|) \quad (14)$$

where X_f is the set of all outliers, $s(x)$ is the DMOS or MOS rating of image x , and $f(x)$ is the predicted score after the logistic transform in (12).

Table I summarizes the performance of S_3 and other algorithms on this task. A sharpness estimator aims to simultaneously obtain high CC and SROCC, and low OR and OD. Note that OR and OD were not calculated on TID2008 because the standard deviations between subjects have not yet been released for this database. In addition, note that the results of BLIINDS-II on the LIVE database are not shown in this table because BLIINDS-II uses LIVE for training (see [35]).

In general, S_3 demonstrates the best performance on almost all criteria. BLIINDS-II is very competitive to S_3 ; however, note that BLIINDS-II requires training and S_3 can generate

²The range $2\sigma_s$ contains 95% of all subjective scores for a given image.

TABLE I
OVERALL PERFORMANCE OF S_3 AND OTHER ALGORITHMS ON THE BLURRED IMAGES FROM THE TID2008, LIVE, AND CSIQ DATABASES. BOLD NUMBERS INDICATE THE TWO BEST PERFORMANCES. RESULTS OF BLIINDS-II ON THE LIVE DATABASE ARE NOT SHOWN BECAUSE BLIINDS-II USES LIVE FOR TRAINING

	JNB	CPBD	ST	MMZ	MDWE	BLIINDS-II	S_3
CC							
TID	0.727	0.848	0.621	0.655	0.709	0.842	0.869
LIVE	0.816	0.895	0.704	0.806	0.806		0.943
CSIQ	0.806	0.882	0.689	0.820	0.797	0.910	0.919
SROCC							
TID	0.714	0.854	0.516	0.728	0.717	0.839	0.839
LIVE	0.787	0.919	0.702	0.858	0.804		0.944
CSIQ	0.762	0.886	0.705	0.857	0.770	0.891	0.911
OR							
LIVE	69.0%	62.8%	76.6%	82.8%	65.5%		53.1%
CSIQ	36.7%	37.3%	42.7%	61.3%	34.0%	28.7%	30.7%
OD							
LIVE	710.5	441.9	956.6	1687.5	704.1		285.8
CSIQ	6.283	4.270	10.369	20.493	6.380	3.070	2.599

a local sharpness map.³ Nonetheless, the performance of BLIINDS-II is noteworthy, given that it was designed for no-reference quality assessment of a variety of distortion types. Among the sharpness estimators, the CPBD algorithm yields the second-best performance, except in terms of OR on the CsiQ database where MDWE yields the second-best performance.

C. Monotonic Prediction of Blur Parameter

Another common technique of validating the ability of a sharpness estimator is to examine the algorithm's performance in monotonically predicting increasing amounts of blur applied to the same image (see, e.g., [3] and [37]). To test this monotonic prediction, we used the 29 reference images from the LIVE image database [32]. The 29 original 24-bits/pixel reference images were blurred using a Gaussian filter of size 15×15 pixels and standard deviations of $\sigma = \{0.4, 0.8, 1.2, 1.6, 2.0, 2.4, 2.8\}$. We then computed S_3 indices for these blurred images.

The results of this test are shown in Fig. 10, in which the S_3 indices for blurred versions of the same original image are represented by individual lines plotted against σ . The average of these data is shown by the solid black line. The same process was applied to five sharpness algorithms: JNB [4], CPBD [21], MMZ [26], ST [2], and MDWE [3].

For any of the 29 given images, the six algorithms all indeed obtain a monotonic trend of sharpness versus σ . Thus, all algorithms are able to correctly rank-order the various blurred versions of the same image. The prediction from S_3 also shows a small variation between curves, which accurately reflects the reduction in sharpness evident when one visually examines these blurred images; these data suggest that S_3 can perform well at rank-ordering blurred versions of different images.

Notice from the curves of S_3 that, for $\sigma \geq 1.6$, the S_3 indices are close to zero. This fact agrees with a visual examination of

³As we show in [15], BLIINDS-II does not perform well in generating sharpness maps (when applied in a block-based fashion); this behavior is expected, given that BLIINDS-II was designed for quality assessment rather than sharpness estimation.

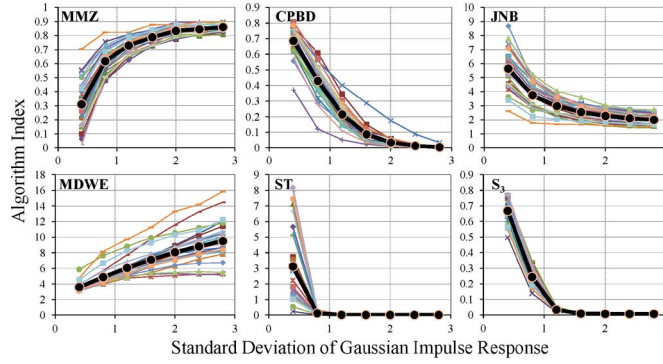


Fig. 10. Relationship between the standard deviation of the Gaussian blurring filter's impulse response and the sharpness/blurriness index of different algorithms. Notice that the curves from S_3 shows relatively small variation which agrees with a visual examination of the blurred images.

these images; visually, the overall sharpnesses of images blurred with $\sigma \geq 1.6$ are all very low and significantly lower than images blurred with $\sigma \leq 1.2$ (see [15]). However, S_3 is still able to discriminate between highly blurred images; the S_3 index of an image with $\sigma = 1.6$ is actually at least 1.5 times greater than the index of the same image with $\sigma = 2.8$.

D. Local Sharpness Prediction

In addition to the index, the S_3 map can be very useful for a variety of applications, e.g., local autoenhancement algorithm [2] and main subject detection [5], because of its ability to measure locally the perceived sharpness of each region in an image. In this section, we describe a subjective experiment to create ground-truth sharpness maps of six images. The S_3 maps of these images are then compared to the ground-truth maps to validate the local performance of S_3 .

1) Experiment Design: Six color images of size 300×400 pixels were chosen to generate subjective sharpness maps. Stimuli were displayed on a LaCie 324 24-in liquid-crystal display monitor (1920×1200 at 60 Hz). The display yielded minimum and maximum luminances of 0.80 and 259 cd/m^2 , respectively, with a luminance gamma of $\gamma = 2.2$. Stimuli were viewed binocularly through natural pupils in a darkened room at a distance of approximately 60 cm. Eleven adult subjects, both male and female whose ages ranged from 23 to 30, took part in the experiment. All had self-reported normal or corrected-to-normal visual acuity.

In the experiment interface, which is shown in [15], two versions of the same image were displayed against a mid-gray background. The left image was divided into blocks of size 16×16 , and the same image (without block division) was displayed on the right-hand side for reference. Subjects rated the sharpness of each block by using an integer scale from 1 to 3, where 1 denoted that the block was very sharp, 3 denoted that the block was not sharp, and 2 was anything in between. The testing interface contained options to assign a sharpness level to multiple blocks and to undo an assignment, which facilitated the testing.

For each image, subjects performed the experiment twice; in the second trial, the grid was offset by 8 pixels both horizontally and vertically. The two resulting maps were then averaged

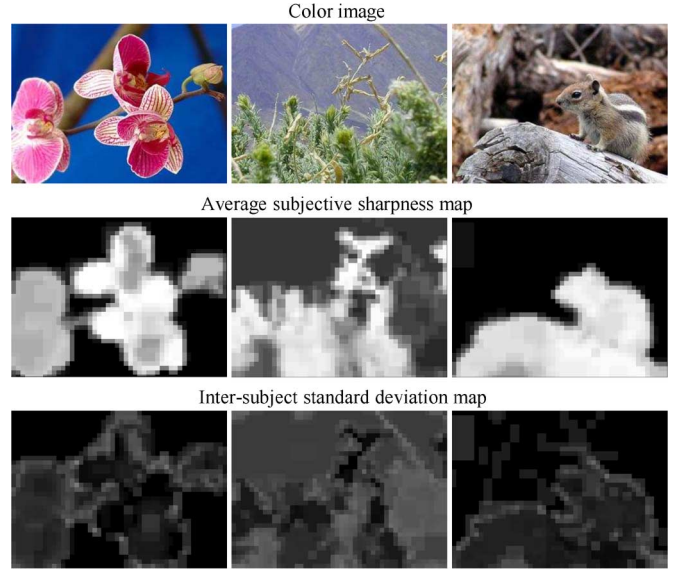


Fig. 11. Color images, their corresponding average subjective sharpness maps, and the intersubject standard deviation maps.

to make a single map and thus provide a sharpness map with an 8×8 block size. In comparison to the method of rating every 8×8 block, in which there were 1800 blocks for each image, this method reduced by half the number of blocks rated by each subject, and it also achieved the resolution of 8×8 -pixel blocks for the final subjective sharpness maps. On average, each subject took approximately 10 min to finish one map (one trial).

2) Experiment Results: For each input image, the sharpness ratings were averaged across two trials and across all subjects. The resulting ground-truth sharpness maps contained at least 206 and at most 245 different sharpness levels. Fig. 11 shows the ground-truth sharpness maps and the intersubject standard deviation maps of three images. (The maps of all six images are shown in [15].) Overall, the 11 subjects highly agreed with each other: The linear CCs between average maps and each subject's maps were 0.89 or higher. The standard deviation maps also show low deviation across ratings from different subjects.

3) Performance: We compared the S_3 maps of the six images to the ground-truth maps. Again, the five sharpness algorithms JNB, CPBD, ST, MMZ, and MDWE were used in this comparison. Because none of these latter algorithms directly output a map, we ran the algorithms in a block-based fashion to generate sharpness maps. The input to the algorithms, instead of being the whole image, was each block of the image.

As described in [4] and [21], JNB and CPBD require the smallest block size to be 64×64 . We divided the input image into blocks of size 64×64 with 56 pixels of overlap between neighboring blocks; the sharpness maps from JNB and CPBD therefore have a block size of 8×8 . Three algorithms, i.e., ST, MMZ, and MDWE, were applied to each 32×32 block with 24 pixels of overlap between neighboring blocks; the resulting sharpness maps thus also have the block size of 8×8 .

Fig. 12 shows the maps from the six algorithms on the images *dragon* and *flower*. To promote visibility, each map has been normalized to occupy the range [0–1]. Other algorithms do not generate accurate sharpness maps for the image *dragon*,

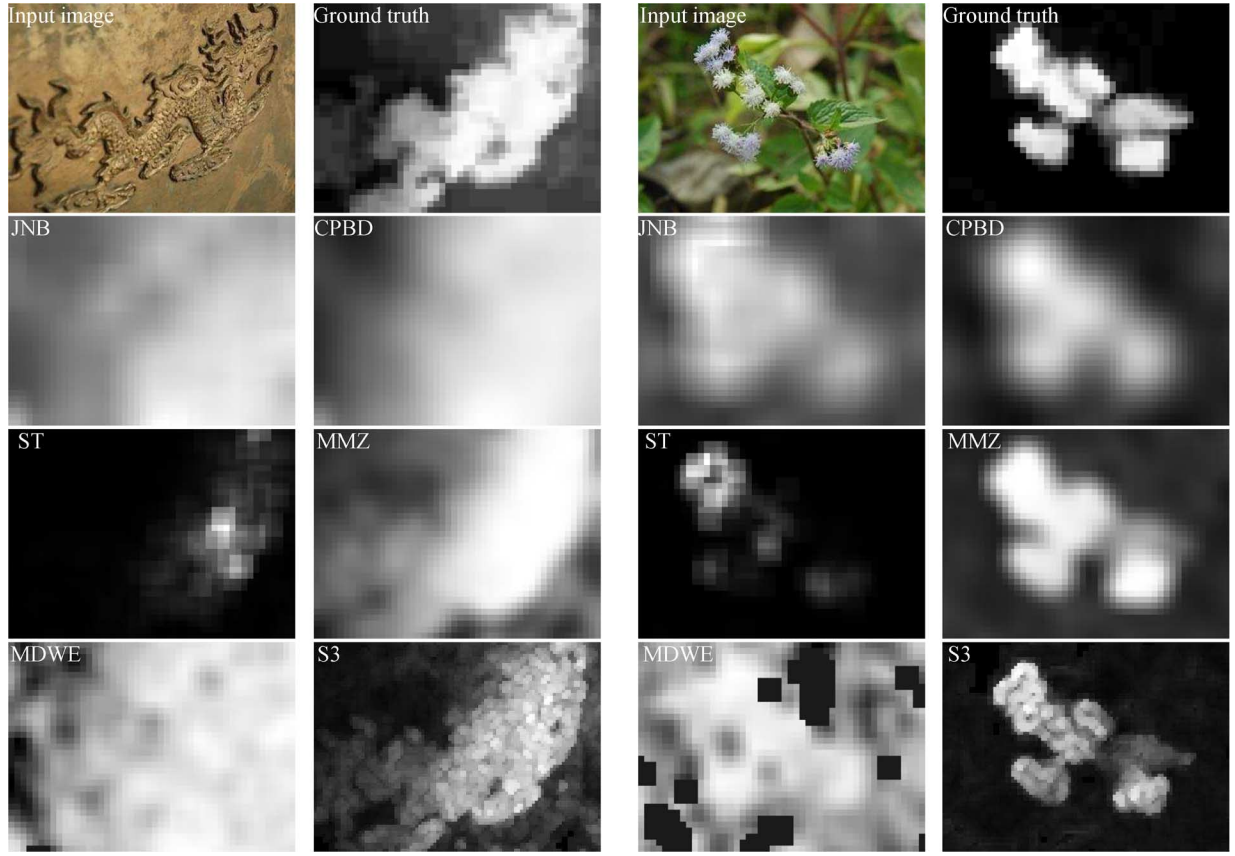


Fig. 12. Comparison of sharpness maps from different algorithms. Black blocks in the MDWE maps are blocks on which MDWE failed to run.

but CPBD and MMZ perform quite well for the image *flower*. In general, S_3 yields the best estimation of the ground truth maps. Note that this is not quite a fair comparison since the other algorithms were not designed to generate a sharpness map. There may certainly be more optimal techniques of applying these estimators locally rather than via the block-based fashion employed here.

We evaluate the performances of S_3 and other algorithms on the entire set of six images using three criteria: CC, SROCC, and Kullback–Leibler divergence (KLD) [38]. The KLD measures the difference between two probability density functions p and q and is given by

$$KLD(p|q) = \sum_x p(x) \log \left(\frac{p(x)}{q(x)} \right). \quad (15)$$

Here, the probability density function generated from the histogram of the ground-truth map was treated as p , and the probability density function generated from the histogram of the predicted map was treated as q . The main challenge in map prediction is to simultaneously obtain high CC and SROCC, and low KLD. Note that, before evaluating the performance of each algorithm, the logistic transform in (12) was also applied to the local sharpness values.

Table II shows the performances of the algorithms on the entire set of six images. As can be seen from this table, in terms of CC, S_3 clearly outperforms all other algorithms, except for the image *monkey*. (The best is from MMZ.) In terms of SROCC and KLD, S_3 gives the best performance for the images *dragon*,

TABLE II
OVERALL PERFORMANCE OF S_3 AND OTHER ALGORITHMS ON THE ENTIRE SET OF SIX IMAGES IN OUR EXPERIMENT. THE BEST TWO PERFORMANCE ARE BOLDED

		JNB	CPBD	ST	MMZ	MDWE	S_3
CC	Dragon	0.629	0.663	0.834	0.862	0.611	0.946
	Flower	0.665	0.858	0.696	0.873	0.761	0.935
	Monkey	0.428	0.495	0.517	0.940	0.276	0.920
	Orchid	0.500	0.831	0.814	0.868	0.097	0.943
	Peak	0.139	0.273	0.875	0.881	0.575	0.926
	Squirrel	0.849	0.935	0.905	0.942	0.852	0.958
	Average	0.535	0.676	0.773	0.894	0.529	0.938
SROCC	Dragon	0.589	0.646	0.866	0.892	0.606	0.930
	Flower	0.706	0.756	0.643	0.547	0.631	0.739
	Monkey	0.313	0.506	0.529	0.885	0.049	0.930
	Orchid	0.439	0.796	0.759	0.841	0.409	0.914
	Peak	0.202	0.052	0.860	0.881	0.490	0.901
	Squirrel	0.835	0.829	0.704	0.801	0.684	0.799
	Average	0.514	0.598	0.727	0.808	0.478	0.869
KLD	Dragon	2.595	2.373	1.890	1.796	2.712	1.550
	Flower	3.530	2.079	3.780	3.398	2.030	2.953
	Monkey	3.129	2.679	2.755	1.158	1.827	0.610
	Orchid	2.545	1.662	2.728	1.844	1.589	0.986
	Peak	1.764	3.003	2.411	2.041	2.484	0.764
	Squirrel	2.657	2.382	3.001	2.248	2.541	3.216
	Average	2.703	2.363	2.761	2.081	2.197	1.680

monkey, *orchid*, and *peak*, and is the second best for the image *flower*. (The best is from CPBD.) The MMZ algorithm generally stands as the second best overall. Nonetheless, the performances of all of the other algorithms are noteworthy, given that none were designed to generate a map.

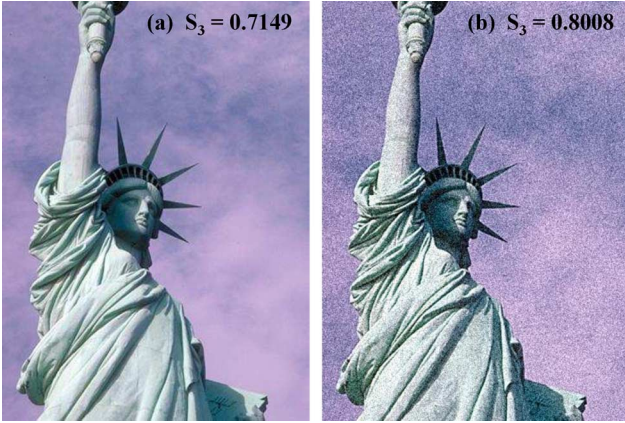


Fig. 13. Noise spreads out over the entire image and makes the image appear sharper. Gaussian white noise was added to (a) to generate (b). (a) $S_3 = 0.7149$. (b) $S_3 = 0.8008$.

E. Effect of Noise

Finally, we briefly discuss the response of the S_3 index when Gaussian white noise is added to the image. Most commonly, additive Gaussian white noise spreads out over the entire image or a large part of the image, which has been shown via psychophysical testing to make the image appear sharper [39], [40]. The perceived sharpness of the noisy image arises mostly from the noise itself, which appears very sharp, as discussed in Section I. An example of this case is shown in Fig. 13, in which Gaussian white noise has been added to the image in Fig. 13(a) to generate the image in Fig. 13(b). Note that, in terms of *image quality*, the image in (b) is distorted and thus has a lower quality than the image in (a). However, in terms of *image sharpness*, the image in (b), whose perceived sharpness is affected by the sharp noise, appears much sharper than the image in (a). The S_3 indices of the two images support this latter observation. (The reader may need to view the images on-screen to appreciate the change in apparent sharpness.)

However, there are cases in which Gaussian white noise is added locally to a small patch and thus does not affect the perceived sharpness of the image. An example of this case is shown in Fig. 14. The image in Fig. 14(b) was generated from the original *monarch* image in Fig. 14(a) by adding a patch of Gaussian white noise, a closeup of which is shown in Fig. 14(c). Although the noisy region does indeed look sharp, the perceived sharpness of the full-sized image is relatively unaffected by the local noise.

When looking at two images to estimate which one is sharper, the image that appears sharper is not necessarily the one that contains more sharp regions. Instead, visual summation dictates that the overall sharpness is determined based on the sharpest region in each image. Previously, in [41], we computed the overall sharpness of an image as the maximum value of its sharpness map, i.e., $S_3 = \max_{x \in X}(S_3(x))$. However, this max operator can be sensitive to spurious sharp locations due to noise. Our proposed computation of the S_3 index via (11) solves this problem, as demonstrated in Fig. 14. The algorithm gives fairly close sharpness values to the two images, which agrees with their perceived sharpnesses.

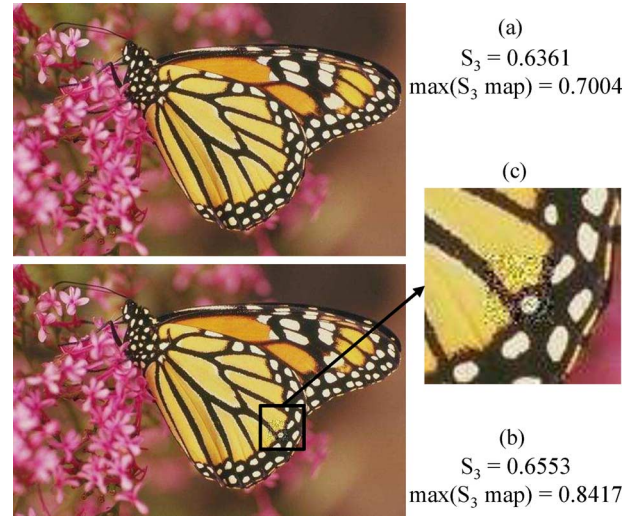


Fig. 14. Example where the max operator is sensitive to spurious sharp locations due to spatially localized noise.

V. CONCLUSION

In this paper, we have presented the algorithm S_3 designed to measure local perceived sharpness in images. By using both spectral and spatial properties, the proposed S_3 measure has been able to quantify local perceived sharpness within and across images. We have also demonstrated that the resulting sharpness map can be collapsed into a scalar index, which quantifies an image's overall perceived sharpness. The utility of this index has been demonstrated for both no-reference quality assessment of blurred images and monotonic estimation of the standard deviation of the impulse response used in Gaussian blurring. We have further demonstrated the accuracy of S_3 in local sharpness estimation by comparing S_3 maps to sharpness maps generated by human subjects. Results have shown that our S_3 maps are highly correlated with the ground-truth sharpness maps. The ground-truth maps, along with further results, can be obtained from [15].

REFERENCES

- [1] G. C. Higgins and L. A. Jones, "The nature and evaluation of the sharpness of photographic images," *J. Soc. Motion Picture Television Eng.*, vol. 58, no. 4, pp. 277–290, 1952.
- [2] D. Shaked and I. Tastl, "Sharpness measure: Towards automatic image enhancement," in *Proc. IEEE Int. Conf. Image Process.*, Sep. 2005, vol. 1, pp. I-937–I-940.
- [3] P. Marziliano, F. Dufaux, S. Winkler, T. Ebrahimi, and G. Sa, "A no-reference perceptual blur metric," in *Proc. IEEE Int. Conf. Image Process.*, 2002, pp. 57–60.
- [4] R. Ferzli and L. J. Karam, "A no-reference objective image sharpness metric based on the notion of just noticeable blur (JNB)," *IEEE Trans. Image Process.*, vol. 18, no. 4, pp. 717–728, Apr. 2009.
- [5] C. Vu and D. M. Chandler, "Main subject detection via adaptive feature refinement," *J. Electron. Imag.*, vol. 20, no. 1, p. 013011, Jan.–Mar. 2011.
- [6] J. Caviedes and S. Gurbuz, "No-reference sharpness metric based on local edge kurtosis," in *Proc. IEEE Int. Conf. Image Process.*, 2002, vol. 3, pp. III-53–III-56.
- [7] N. K. Chern, P. A. Neow, and M. H. Ang, Jr., "Practical issues in pixel-based autofocusing for machine vision," in *Proc. IEEE Int. Conf. Robot. Autom.*, 2001, vol. 3, pp. 2791–2796.
- [8] C. Y. Wee and R. Paramesran, "Image sharpness measure using eigenvalues," in *Proc. 9th ICSP*, 2008, pp. 840–843.

- [9] D. J. Field and N. Brady, "Visual sensitivity, blur and the sources of variability in the amplitude spectra of natural scenes," *Vis. Res.*, vol. 37, no. 23, pp. 3367–3383, Dec. 1997.
- [10] L. I. Rudin, S. Osher, and E. Fatemi, "Nonlinear total variation based noise removal algorithms," *Phys. D*, vol. 60, no. 1–4, pp. 259–268, Nov. 1992.
- [11] G. Blanchet, L. Moisan, and B. Rouge, "Measuring the global phase coherence of an image," in *Proc. 15th IEEE ICIP*, Oct. 2008, pp. 1176–1179.
- [12] D. J. Field, "Relations between the statistics of natural images and the response properties of cortical cells," *J. Opt. Soc. Amer. A*, vol. 4, no. 12, pp. 2379–2394, Dec. 1987.
- [13] D. C. Knill, D. J. Field, and D. Kersten, "Human discrimination of fractal images," *J. Opt. Soc. Amer. A*, vol. 7, no. 6, pp. 1113–1123, Jun. 1990.
- [14] G. M. Johnson and M. D. Fairchild, "Sharpness rules," in *Proc. IS&T/SID 8th Color Imag. Conf.*, 2000, pp. 24–30.
- [15] S₃: A spectral and spatial measure of local perceived sharpness in natural images. Online supplement. [Online]. Available: <http://vision.okstate.edu/s3>
- [16] E. Ong, W. Lin, Z. Lu, X. Yang, S. Yao, F. Pan, L. Jiang, and F. Moschetti, "A no-reference quality metric for measuring image blur," in *Proc. 7th Int. Symp. Signal Process. Appl.*, 2003, vol. 1, pp. 469–472.
- [17] J. Dijk, M. van Ginkel, R. J. van Asselt, L. J. van Vliet, and P. W. Verbeek, "A new sharpness measure based on Gaussian lines and edges," in *Proc. 8th Annu. Conf. Adv. Sch. Comput. Imag.*, 2003, pp. 149–156.
- [18] Y. C. Chung, J. M. Wang, R. R. Bailey, S. W. Chen, and S. L. Chang, "A non-parametric blur measure based on edge analysis for image processing applications," in *Proc. IEEE Conf. Cybern. Intell. Syst.*, 2004, vol. 1, pp. 356–360.
- [19] S. Wu, W. Lin, L. Jian, W. Xiong, and L. Chen, "An objective out-of-focus blur measurement," in *Proc. 5th Int. Conf. Inf. Commun. Signal Process.*, 2005, pp. 334–338.
- [20] S. Zhong, Y. Liu, Y. Liu, and F. Chung, "A semantic no-reference image sharpness metric based on top-down and bottom-up saliency map modeling," in *Proc. 17th IEEE ICIP*, 2010, pp. 1553–1556.
- [21] N. D. Narvekar and L. J. Karam, "A no-reference perceptual image sharpness metric based on a cumulative probability of blur detection," in *Proc. Int. Workshop QoMEx*, 2009, pp. 87–91.
- [22] X. Zhu and P. Milanfar, "A no-reference sharpness metric sensitive to blur and noise," in *Proc. 1st Int. Workshop QoMEX*, 2009, pp. 64–69.
- [23] F. Crete, T. Dolmire, P. Ladret, and M. Nicolas, "The blur effect: Perception and estimation with a new no-reference perceptual blur metric," in *Proc. SPIE—Electronic Imaging Symp. Conf. Human Vision and Electronic Imaging*, San Jose, CA, 2007, vol. XII, p. EI 6492–16.
- [24] E. Tsomko and H. J. Kim, "Efficient method of detecting globally blurry or sharp images," in *Proc. Int. Workshop Image Anal. Multimedia Interactive Services*, 2008, pp. 171–174.
- [25] L. Debing, C. Zhibo, M. Huadong, X. Feng, and G. Xiaodong, "No reference block based blur detection," in *Proc. Int. Workshop QoMEx*, 2009, pp. 75–80.
- [26] X. Marichal, W. Y. Ma, and H. J. Zhang, "Blur determination in the compressed domain using dct information," in *Proc. IEEE Int. Conf. Image Process.*, 1999, vol. 2, pp. 386–390.
- [27] N. Zhang, A. Vladar, M. Postek, and B. Larrabee, "A kurtosis-based statistical measure for two-dimensional processes and its application to image sharpness," in *Proc. Section Phys. Eng. Sci. Amer. Statist. Soc.*, 2003, pp. 4730–4736.
- [28] M. K. Janez and S. Kovacic, "A Bayes-spectral-entropy-based measure of camera focus using a discrete cosine transform," *Pattern Recognit. Lett.*, vol. 27, no. 13, pp. 1431–1439, Oct. 2006.
- [29] R. Hassen, Z. Wang, and M. Salama, "No-reference image sharpness assessment based on local phase coherence measurement," in *Proc. IEEE ICASSP*, Mar. 2010, pp. 2434–2437.
- [30] D. J. Graham, D. M. Chandler, and D. J. Field, "Can the theory of "whitening" explain the center-surround properties of retinal ganglion cell receptive fields?," *Vis. Res.*, vol. 46, no. 18, pp. 2901–2913, Sep. 2006.
- [31] N. Graham, *Visual Pattern Analyzers*. New York: Oxford Univ. Press, 1989.
- [32] H. R. Sheikh, Z. Wang, A. C. Bovik, and L. K. Cormack, Image and video quality assessment research at LIVE. [Online]. Available: <http://live.ece.utexas.edu/research/quality/>
- [33] E. C. Larson and D. M. Chandler, "Most apparent distortion: Full-reference image quality assessment and the role of strategy," *J. Electron. Imag.*, vol. 19, no. 1, p. 011006, Jan.–Mar. 2010.
- [34] N. Ponomarenko, V. Lukin, A. Zelensky, K. Egiazarian, M. Carli, and F. Battisti, "TID2008 - A database for evaluation of full-reference visual quality assessment metrics," *Adv. Modern Radioelectron.*, vol. 10, pp. 30–45, 2009.
- [35] M. A. Saad, A. C. Bovik, and C. Charrier, "Model-based blind image quality assessment using natural DCT statistics," *IEEE Trans. Image Process.*, 2011, to be published.
- [36] "Final Report from the Video Quality Experts Group on the Validation of Objective Models of Video Quality Assessment, Phase II," VQEG, Aug. 2003 [Online]. Available: <http://www.vqeg.org>
- [37] R. Ferzli and L. J. Karam, "Human visual system based no-reference objective image sharpness metric," in *Proc. IEEE Int. Conf. Image Process.*, Oct. 2006, pp. 2949–2952.
- [38] T. M. Cover and J. A. Thomas, *Elements of Information Theory*, 2nd ed. New York: Wiley-Interscience, Aug. 2006.
- [39] V. Kayargadde and J. B. Martens, "Perceptual characterization of images degraded by blur and noise: Experiments," *J. Opt. Soc. Amer. A*, vol. 13, no. 6, pp. 1166–1177, Jun. 1996.
- [40] S. S. Hemami, D. M. Chandler, and K. H. Lim, "Effects of spatial correlations and global precedence on the visual fidelity of distorted images," in *Proc. Human Vis. Electron. Imag.*, 2006, pp. 1–15.
- [41] C. Vu and D. M. Chandler, "S₃: A spectral and spatial sharpness measure," in *Proc. 1st Int. Conf. Adv. Multimedia*, 2009, pp. 37–43.



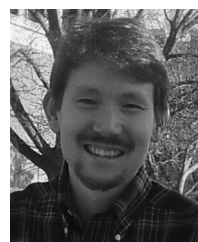
Cuong T. Vu received the B.S. degree in telecommunications from the Posts and Telecommunications Institute of Technology, Vietnam, in 2005. He is currently working toward the Ph.D. degree in electrical and computer engineering in the School of Electrical and Computer Engineering, Oklahoma State University, Stillwater, where he specializes in image processing and perception.

His research interests include coding and analysis of visual information and image quality assessment.



Thien D. Phan received the B.S. degree in information technology from Hanoi University of Technology, Hanoi, Vietnam, in 2008. He is currently working toward the Ph.D. degree in the School of Electrical and Computer Engineering, Oklahoma State University, Stillwater.

His research interests include image processing, computer vision, data compression, machine learning, and optimization for multidimensional signal-processing applications.



Damon M. Chandler received the B.S. degree in biomedical engineering from The Johns Hopkins University, Baltimore, MD, in 1998 and the M.Eng., M.S., and Ph.D. degrees in electrical engineering from Cornell University, Ithaca, NY, in 2000, 2003, and 2005, respectively.

From 2005 to 2006, he was a Postdoctoral Research Associate with the Department of Psychology, Cornell University. He is currently an Assistant Professor with the School of Electrical and Computer Engineering, Oklahoma State University, Stillwater, where he heads the Laboratory of Computational Perception and Image Quality. His research interests include image processing, data compression, computational vision, natural scene statistics, and visual perception.

where he heads the Laboratory of Computational Perception and Image Quality. His research interests include image processing, data compression, computational vision, natural scene statistics, and visual perception.